

RESEARCH

Open Access



# Aggravated liver steatosis in a modern dietary mouse model via long-term treatment of SiO<sub>2</sub> nanoparticles in drinking water

Tzung Cheng Ye<sup>1</sup>, Shu-Ju Chao<sup>1</sup>, Chihpin Huang<sup>1\*</sup>  and Ru-Tsun Mai<sup>2</sup>

## Abstract

SiO<sub>2</sub> nanoparticles (SNPs), which are abundant in water and are used for various applications, for example, as food additives and anticaking agents, are of growing concern because of rising exposure to human health. Research has reported low potential side effects in animal models treated with SNPs; however, a few in vivo studies have shown cause for concern. Presently, high-fat foods have changed our lives and increased the incidence rates of fatty liver, obesity, and overweight, and high-fat foods issue is prevalent in our modern society. To understand the rising SNPs exposure in life and modern dietary habits combined effect, we design experiments to study this research.

Institute of Cancer Research mice fed a normal or high-fat diet were treated with different concentrations of SNPs for long-term effects. Blood and liver tissue were collected and prepared for blood biochemical assays, histology analysis, silicon and triglycerides (TGs) accumulation, immunohistochemistry, fibrosis staining, and terminal deoxynucleotidyl transferase dUTP nick-end labeling staining to analyze the influence of the combination of SNPs and a high-fat diet.

This research found that the presence of SNPs in drinking water with the consumption of a high-fat diet was associated with the accumulation of SNPs and TGs in liver tissue, elevated aspartate aminotransferase and alanine aminotransferase levels in serum, activation of fibrosis and inflammation, increased oxidative stress through 4-hydroxynonenal, and the development of liver steatosis. The results showed that the long-term effect of SNPs in drinking water might induce liver steatosis, particularly under modern dietary habits such as a high-fat diet. This study investigated the interactions between environmental nanoparticles, such as the long-term risk of exposure to SNPs, and dietary factors, suggesting a significant risk to liver health, especially in human health.

**Keywords** Drinking water, High-fat diet, Normal diet, Nanoparticles, Fatty liver, Steatosis

## 1 Introduction

Dietary habits lead to various health effects. Sedentary lifestyles, infrequent exercise, and the transformation of modern nutritional patterns, especially regarding the popularity of refined foods, sugary beverages, and fast food, have led to reduced daily calorie requirements and overconsumption. When daily calorie intake exceeds the daily calorie requirement, the liver tissue converts unused calories into glycogen for temporary storage in the liver and skeletal muscle or into fat accumulated in the liver, leading to fatty liver, obesity, and overweight

\*Correspondence:

Chihpin Huang  
huang@nycu.edu.tw

<sup>1</sup> Institute of Environmental Engineering, National Yang Ming Chiao Tung University, Hsinchu 300093, Taiwan

<sup>2</sup> Department of Biological Science & Technology, National Yang Ming Chiao Tung University, Hsinchu 300193, Taiwan



© The Author(s) 2024. **Open Access** This article is licensed under a Creative Commons Attribution 4.0 International License, which permits use, sharing, adaptation, distribution and reproduction in any medium or format, as long as you give appropriate credit to the original author(s) and the source, provide a link to the Creative Commons licence, and indicate if changes were made. The images or other third party material in this article are included in the article's Creative Commons licence, unless indicated otherwise in a credit line to the material. If material is not included in the article's Creative Commons licence and your intended use is not permitted by statutory regulation or exceeds the permitted use, you will need to obtain permission directly from the copyright holder. To view a copy of this licence, visit <http://creativecommons.org/licenses/by/4.0/>.

[1–3]. According to statistics from the Ministry of Health Services in Taiwan, rates of obesity and overweight, which lead to fatty liver, cirrhosis, and liver cancer, are increasing yearly. Hence, the evidence shows that modern nutritional patterns are an important factor related to liver function. The liver, the largest organ in the body, has the function of detoxification and is also a key site for nanoparticle accumulation [2–4]. Nonalcoholic fatty liver disease, a common cause of chronic liver disease that includes a range of presentations such as simple steatosis, fibrosis, cirrhosis, and hepatocytic carcinoma [2, 3, 5–7], is characterized by abnormally accumulated lipids and liver steatosis due to modern dietary habits, and its pathogenesis and progression are still incompletely understood. In addition, studies have reported that mouse models fed with a high-fat diet have similar pathological features as patients with fatty liver [2, 8, 9].

Many researchers have reported the correlation between the quality of drinking water and diseases such as those related to embryo development, neurodegeneration, cardiovascular disease, and obesity [10, 11]. One of the key roles of drinking water treatment plants is particle removal following the process of coagulation, flocculation, and sedimentation [12, 13]. Although the turbidity of drinking water must be lower than 2 NTU according to most drinking water regulations, such a low turbidity of water still contains many nanoparticles (NPs) such as SiO<sub>2</sub> NPs (SNPs) [12, 13]. SNPs are the most common inorganic NPs and are used in different areas. For instance, manufacturers use SNPs to produce many daily necessities, from glass to semiconductors. SNPs are used as anticaking and additive agents in the food industry. Adding SNPs to foods allows for long-term preservation and lengthened shelf-life, helps powdered ingredients stick together, protects against the effects of moisture, and allows liquid food to flow smoothly [14, 15]. In sterile bulk food-grade SNPs, the concentration of SNPs is in the range of 2 to 200 mg SNPs per serving size [14, 15]. SiO<sub>2</sub> is considered biocompatible; however, the gradually increasing use of SNPs in a wide variety of applications, including engineering, biomedicine, agriculture, and cosmetics, has increased the chances of chronic exposure and growing concern in the potential long-term risks to human health in our lives [7, 16–20]. Increasing toxicological evidence has demonstrated that SNPs cause liver damage and induce oxidative stress, apoptosis, inflammation, fibrosis, etc. [17, 19, 21–26]. In addition, increased lactate dehydrogenase levels, rates of liver cell necrosis, hepatocytic swelling, and fatty liver induces were also found in a mouse model exposed to SNPs [27]. The effects of SNPs on various cell lines include cellular cytotoxicity, reactive oxidative stress, apoptosis induction, mitochondrial damage, and DNA damage [28–30].

Several experiments have shown that the uptake of NPs changes fatty liver indices, such as aspartate aminotransferase (AST) and alanine aminotransferase (ALT) levels, in serum [20, 25, 27, 31]. The relatively small size of SNPs compared to other SNPs could induce higher serum levels of AST and ALT in mouse models [32]. Global proteomics showed that the SNPs exposure was related to cytotoxicity and lipid metabolism [33]. The evidence revealed that exposure to SNPs might affect liver function and fat accumulation in liver tissue. However, those studies focused on the short-term effects of daily NP treatment by oral gavage or tail vein administration for less than two months [4, 21, 27, 34]. The long-term impact of SNP exposure is still unclear.

The rising long-term exposure to SNPs in our lives and the evidence of induced liver steatosis through SNPs in cell lines [28–30], proteomics [33], and mice models [4, 21, 27, 34] reveal that SNPs may play a crucial role in the liver. The modern dietary habits, which uptake more high-fat food, are highly related to liver steatosis [2, 8, 9]. Both SNPs and high-fat food show similar evidence of liver steatosis. However, little evidence shows the relationship between long-term exposure to SNPs and high-fat food. Therefore, Institute of Cancer Research (ICR) mice models were used in our research to understand the increasing chronic exposure risk to SNPs, which exacerbates liver damage under modern dietary habits in contemporary society and may give the widespread use of SNPs in various applications and their potential health implications. ICR mice are the most commonly used outbred mice stock and are often used in cancer trials and drug screening because of the strain heterozygosity, convenient management of feeding, short life cycle, and high similarity of genetics to Homo species. In our ICR mouse model, mice were treated with either a normal diet (ND) or a high-fat diet (HFD) and different concentrations of SNPs by oral gavage to mimic long-term exposure in drinking water for 25 weeks. Histology, accumulation of silicon and triacylglycerol in tissue, blood biochemical assays, picosirius red/Masson trichrome staining, terminal deoxynucleotidyl transferase dUTP nick end labeling (TUNEL) staining, and immunohistochemical staining were used to determine the correlation between long-term treatment of SNPs in drinking water and modern dietary habits in our model.

## 2 Materials and methods

### 2.1 Materials

40 nm SiO<sub>2</sub> nanoparticles were purchased from UniRegion Bio-Tech. Male Bltw: CD1 (ICR) mice, which were 20–26 g in weight at eight weeks of age, ND (AIN-93G Diet), which contained 16.7% of calories from fat, and HFD (High-fat AIN-93G purified Rodent Diet), which

contained 52.4% of calories from fat were purchased from BioLASCO Taiwan Co. Isoflurane (Cat. No. 792632), formalin (Cat. No. 47608), hydrofluoric acid (Cat. No. 7664-39-3), Tween-20 (Cat. No. 9005-64-05), Ethanol (Cat. No. 64-17-5), xylene (Cat. No. 1330-20-7), Mounting medium (Cat. No. 06522), trisodium salt dihydrate (Cat. No. 6132-04-3), Masson's trichrome staining kit (Cat. No. HT15), TUNEL assay kit (Cat. No. S7101) were obtained from Sigma-Aldrich. Hydrogen peroxide (Cat. No. 31642) was acquired from Fluka-Honeywell. Lipid extraction kit (Cat. No. K216-50) was purchased from BioVision. Peroxidase (Cat. No. 31487) was received from Thermo Scientific. The hematoxylin and eosin staining kit (H&E) (Cat. No. H2502) was obtained from vector laboratories. Cluster of differentiation 3 (CD3) antibody (EMD Millipore, Cat. No. PC630), 4-hydroxynonenal (4-HNE) antibody (R&D, Cat. No. MAB3249), tumor necrosis factor- $\alpha$  (TNF- $\alpha$ ) antibody (Genetex, Cat. No. GTX110520), and interleukin-6 (IL-6) (Genetex, Cat. No. GTX110527) were prepared for immunohistochemistry (IHC). Picosirius red solution (Cat. No. SRS25) was purchased from Scy Tek. The citric acid solution was prepared with 10 mM trisodium salt dihydrate pH 6.0 and 0.5% Tween-20. The reverse osmosis water (turbidity < 1 NTU) was prepared from a pure water system (Arium 611DI, Sartorius Stedim). TEM grid (PELCO® Center-Marker Grids, 500 mesh, 3.0 mm O.D., Copper) (Cat. No. 1GC500) was purchased from Ted Pella, Inc.

## 2.2 The preparation and characterization of SiO<sub>2</sub> nanoparticles

The different stock concentrations of the 40 nm amorphous SNPs were freshly prepared in reverse osmosis water and sterilized by autoclave at 121 °C for 15 min for each oral gavage in our animal model. 0.01 g of SNPs was diluted by 50 mL of absolute alcohol and vortex for 5 min. One drop of the diluted sample was put on the transmission electron microscopy (TEM) grid and air dry. The

image of the SNPs was obtained by field emission TEM (JELO, JEM-F200) from the National Yang-Ming Chiao Tung University Instrument Resource Center. Image J software (National Institutes of Health, Bethesda, MD) was used to measure the size of the nanoparticles. The hydrodynamic sizes of nanoparticles in reverse osmosis water and the zeta potential were analyzed by a Zetasizer Nano series (Malvern). Purity and endotoxin determination were obtained by Agilent's inductively coupled plasma (ICP) atomic emission spectrometer (Agilent 720, USA) and gel-clot limulus amoebocyte lysate assay, separately.

## 2.3 Animal model

All ICR mice were housed at 21 ± 2 °C, 55–60% humidity, and 12 h light/dark cycle conditions. They were fed an ND or HFD, ad libitum. ICR mice were fed twice per week with different concentrations of SNPs (suspended by vibration for 3 min) and were separated into eight groups ( $n=6$  per group). The detailed experimental conditions are shown in Table 1. In choosing the SNP administration method, oral gavage instead of a water bottle for drinking was used because the SNPs precipitate easily in reverse osmosis water. Therefore, the amount of SNP intake could not be accurately predicted by using a water bottle. Based on previous studies showing that the average concentration of SNPs administered to mice with no outcomes of abnormal behavior or only minor or absence of toxicological findings were observed between 1.0 and 333 mg kg<sup>-1</sup> mouse body weight of SNP treatment concentrations [4, 21, 27, 34], even at very high doses (1–2.5 g kg<sup>-1</sup> body weight d<sup>-1</sup>) [35, 36], the total weekly amount of silica administered we used was lower than the mice's maximum metabolic cycle and the most tolerance of mice. Therefore, we design the treatment of SNPs concentration ranging from 100 to 300 mg kg<sup>-1</sup> mouse body weight twice weekly. Circadian rhythms in liver homeostasis play fundamental roles by regulating glucose and

**Table 1** Conditions of experiment groups of mice

Experiment groups	mice numbers	Diet	SNPs treatment concentrations (mg kg <sup>-1</sup> mice body weight)
ND-SNP0	6	Normal Diet	0 mg kg <sup>-1</sup> (reverse osmosis only)
ND-SNP100	6	Normal Diet	100 mg kg <sup>-1</sup>
ND-SNP200	6	Normal Diet	200 mg kg <sup>-1</sup>
ND-SNP300	6	Normal Diet	300 mg kg <sup>-1</sup>
HFD-SNP0	6	High-fat Diet	0 mg kg <sup>-1</sup> (reverse osmosis only)
HFD-SNP100	6	High-fat Diet	100 mg kg <sup>-1</sup>
HFD-SNP200	6	High-fat Diet	200 mg kg <sup>-1</sup>
HFD-SNP300	6	High-fat Diet	300 mg kg <sup>-1</sup>

lipid metabolism [37–39]. Therefore, we treated the SNPs twice weekly at the exact fixed times each week to decrease the SNPs' metabolism difference through the circadian rhythms effect. Blood was collected from the tail veins of the mice after 6 and 12 weeks of SNP treatment. Mice were sacrificed under 4% isoflurane anesthesia by a gas anesthesia machine, and the liver tissue and blood obtained by heart puncture from the mice exposed to SNPs for 25 weeks were preserved. Blood and liver organs fixed with 10% formalin were subjected to further blood biochemical assays, histopathological examinations, measurements of silicon element and triglyceride (TG) accumulation in the liver, and IHC at the Taiwan Mouse Clinic.

#### 2.4 Serum preparation and blood biochemical assays

The blood was transferred to a BD microtainer<sup>1</sup> (BD, 365967 Gold BD SST<sup>TM</sup>). Blood clotting was allowed to proceed at room temperature for 20–30 min but not for longer than 3 h to circumvent hemolysis. Serum was obtained by centrifuging whole blood at 3,000 rpm for 15 min at 4 °C. The supernatant was transferred to a new 1.5 mL Eppendorf tube, and the serum was stored at –80 °C for future experiments. 10 µL of serum was analyzed directly by a biochemical analyzer (HITACHI 3100 analyzer, Japan) for each liver function-related biomarker, such as high-density lipoprotein cholesterol (HDL-C), low-density lipoprotein cholesterol (LDL), total cholesterol (T-CHO), TG, ALT, and AST [25, 27].

#### 2.5 Histopathological examination

The dissected liver tissues were weighed, photographed, fixed in 10% formalin, embedded in paraffin, sectioned, and stained with H&E staining for histological examination by the Taiwan Mouse Clinic. After H&E staining, the slides with fatty droplet areas were observed by optical microscopy (Nikon, ECLIPSE Ci) and photographed by NIS-Elements BR software (Nikon). 20 images from each mouse were analyzed by Image-Pro software (Total-smart Technology Co., Taichung, Taiwan) to determine each mouse's steatosis percentage.

#### 2.6 Silicon element accumulation in liver tissue

The liver tissues were homogenized in liquid nitrogen. One-half gram of homogeneous liver tissue was digested with 5 mL of hydrofluoric acid at 80 °C for 30 min, and after digestion, the cooled sample was incubated with 1 mL of 30% hydrogen peroxide for complete oxidation at 80 °C for 30 min. The completely oxidized sample was cooled to room temperature and filtered through a 0.45 µm filter. The standard silicon concentration was used for the quantitative standard curve by ICP (Agilent Technologies ICP-OES 700 Series) from the National Yang-Ming

Chiao Tung University Environment Technology & Smart System Research System. The silicon element concentration in each sample was analyzed using ICP and the quantitative standard curve.

#### 2.7 Accumulated TGs in liver tissue

A lipid extraction kit was used to extract TG from liver tissue. Liver tissue (0.5 g) was mixed with 500 µL of lipid extraction buffer and homogenized on ice. The supernatant-containing tube was left open and dried in a 37 °C incubator, and the lipid extract was resuspended in 50 µL of lipid suspension buffer. The lipid extract was sonicated for 10 min at 37 °C. The lipid extract was used for measuring the amount of TG by an automated biochemical analyzer (Hitachi 3100 analyzer, Japan) at the Taiwan Mouse Clinic.

#### 2.8 Liver fibrosis staining

Liver paraffin sections were stained with picosirius red solution or Masson's trichrome staining kit. The sections were deparaffinized with xylene and a series of decreasing ethanol series. The specimen sections were incubated with picosirius red solution or with aniline blue solution for 60 min at room temperature, and the slides were washed with acetic acid solution and absolute alcohol. The slides were dehydrated and mounted. The percentage of the positive staining area was observed by optical microscopy (Nikon, Eclipse Ci) and photographed using NIS-Elements BR software (Nikon). To determine each mouse's fibrosis percentage, 20 images from each mouse were analyzed by Image-Pro software (Total-smart Technology Co., Taichung, Taiwan).

#### 2.9 IHC

For IHC, 8–10 µm of paraffin-embedded tissue samples were deparaffinized with xylene and a series of decreasing ethanol dilutions. The hydrated sections were pretreated with a citric acid solution for 8 min. For non-specific blocking, peroxidase was applied for 10 min at room temperature. After blocking, the slides were stained with the primary antibodies against CD3 at a dilution of 1:500, 4-HNE at a dilution of 1:200, TNF-α at a dilution of 1:200, and IL-6 at a dilution of 1:200 overnight. After primary antibody incubation, the appropriate secondary antibody was applied for 1 h at room temperature. A mounting medium was used to envelop the slides. The percentage of the positive staining area was observed by optical microscopy (Nikon, Eclipse Ci) and photographed using NIS-Elements BR software (Nikon). To determine each mouse's positive areas, 20 images from slides were analyzed using Image-Pro software (Total-smart Technology Co., Taichung, Taiwan).

## 2.10 TUNEL staining

The paraffin sections dewaxed by xylenes and a series of decreasing ethanol series were stained by a TUNEL assay kit to assess liver apoptosis. A proteinase k digestion ( $20 \mu\text{g mL}^{-1}$ ) was carried out for 15 min at room temperature. Endogenous hydrogen peroxidase activity was quenched by 3% hydrogen peroxide. dUTP was added to the FREE 3' -OH break-ends of DNA by terminal deoxynucleotidyl transferase enzyme for 60 min, and the labeled DNA was detected for 30 min using anti-digoxigenin-peroxidase. The application of diaminobenzidine tetrahydrochloride resulted in a brown reaction product. The positively staining cells were observed by optical microscopy (Nikon, Ci) and photographed using NIS-Elements BR software (Nikon). To quantify each mouse's apoptosis cells, 20 slide images from each sample were analyzed using Image-Pro software (Total-smart Technology Co., Taichung, Taiwan).

## 2.11 Statistical analysis

The results are presented as the means  $\pm$  standard errors of the means and were analyzed using SigmaPlot v14.0 software (Systat Software Inc, Palo Alto, CA). Two-way analysis of variance (ANOVA) was used to assess statistically significant differences, which were considered \*,  $p < 0.05$ , \*\*,  $p < 0.005$ , and \*\*\*, and  $p < 0.001$ .

## 3 Results and discussion

### 3.1 Characterization of SiO<sub>2</sub> nanoparticles

TEM was used to characterize the SiO<sub>2</sub> nanoparticles in Fig. S1. The average size of SiO<sub>2</sub> is  $40.8 \pm 5.6$  nm (means  $\pm$  standard error of the means). The hydrodynamic size of SiO<sub>2</sub> nanoparticles in reverse osmosis water is  $390.2 \pm 4.8$  nm (means  $\pm$  standard error of the means). The zeta potential is  $37.5 \pm 0.9$  mV. The morphology is amorphous (Fig. S1). The purity of SNPs was 99.99%. No endotoxin existed in the SNPs.

### 3.2 SNP effects on the body weight and silicon accumulation in the liver

Figure 1a shows the body weight variations in the ICR mice after oral administration of different concentrations of SNPs in the presence of the ND or HFD. All mice tolerated oral gavage doses between 100 to 300

mg kg<sup>-1</sup> twice weekly during the experimental period. The body weights in each group were slightly increased in a time-dependent manner. After 12 weeks of treatment, the body weights were significantly increased in the HFD-SNP0 group compared to those of the ND-SNP0 group ( $p < 0.01$ – $0.05$ , ANOVA) (Fig. 1a). The results showed that HFD led to an increase in body weight after 12 weeks of treatment because the HFD provided higher calorie intake and increased body weight. Within each diet, no statistically significant body weight differences were observed due to the consumption of different dosages of SNPs compared to the respective control (ND-SNP0 or HFD-SNP0), which was treated with reverse osmosis water only ( $p > 0.05$ , ANOVA) (Fig. 1a). Silica was found in natural such as water, soil, plant, and animal [40, 41]. Therefore, both ND-SNP0 and HFD-SNP0 had silicon accumulation in the liver (Fig. 1b) because it is from the silicon naturally present in the mouse liver. During the experimental period, no abnormal behavior, such as labored breathing or arching of the back; no clinical signs, such as bloating and vomiting; and no induced apparent toxicity were noted. After sacrifice at the end of 25 weeks, no visible changes in organ morphology were observed. Therefore, simulated SNPs had no immediate or noticeable impact on our mouse model, similar to previous research [35, 36].

ICP, a method for quantifying specific elements present samples, was used to quantify the average silicon accumulation (mg silicon g<sup>-1</sup> liver). The amount of silicon in the livers of mice in the ND groups showed no significant differences ( $p > 0.05$ , ANOVA) compared with ND-SNP0, except in the ND-SNP300 groups ( $p < 0.05$ , ANOVA) (Fig. 1b). With the increasing doses of SNPs, silicon accumulation levels in the HFD groups were significantly increased ( $p < 0.001$ – $0.05$ , ANOVA) (Fig. 1b). The relative extent of accumulated silicon in the ND-SNP300 group was significantly increased compared with those of the HFD-SNP300 group ( $p < 0.001$ , ANOVA) (Fig. 1b). Our results further demonstrated that an HFD deteriorated silicon accumulation in the liver; likewise, in previous research, the main silicon accumulated in liver tissue [4, 7, 40].

(See figure on next page.)

**Fig. 1** Body weight change in the experimental period and silicon accumulation in the liver. Body weight changes in mice treated with 0, 100, 200, or 300 mg of SNPs kg<sup>-1</sup> mouse body weight by oral gavage twice per week in the presence of an ND or HFD (a). Each point represents the means  $\pm$  standard error of the means ( $n = 6$ ). \*,  $p < 0.05$  and \*\*,  $p < 0.01$  when the HFD-SNP0 group was compared with the ND-SNP0 groups using ANOVA. Body weight differences were observed in the ND and HFD mice fed with distinct SNPs ( $p > 0.05$ , ANOVA). No significance (n.s.). Silicon accumulation in liver tissue (mg silicon g<sup>-1</sup> liver) was measured at 25 weeks by ICP (b). Data are expressed as the means  $\pm$  standard error of the means ( $n = 6$ ). #,  $p < 0.001$  when the HFD-SNP300 group was compared with the ND-SNP300 group using ANOVA

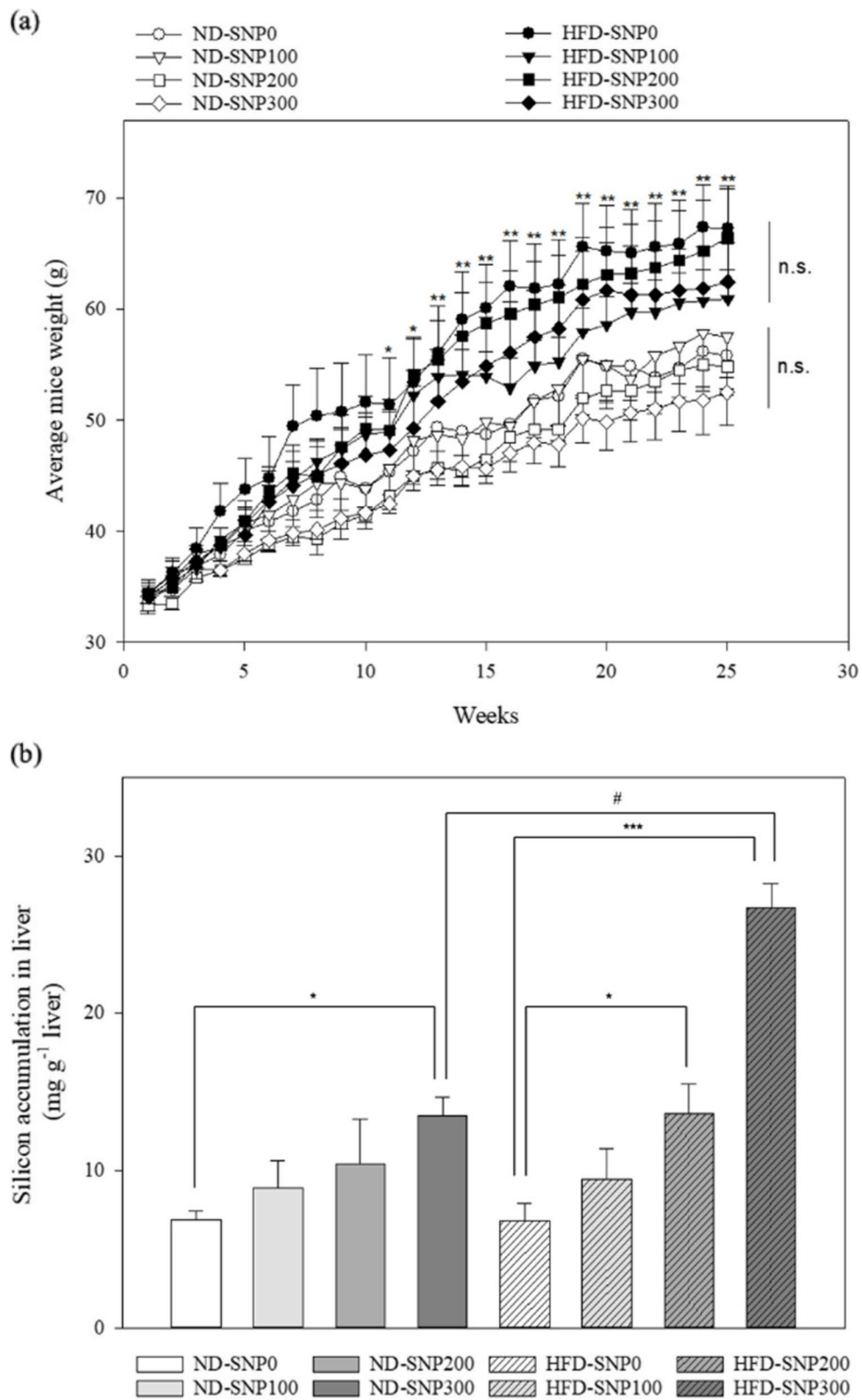


**Fig. 1** (See legend on previous page.)

### 3.3 Liver degeneration due to a combination of SNPs and HFD treatment

Mice were maintained on the ND or HFD with different dosages of SNPs until they were sacrificed at 25 weeks. To determine indices of liver degeneration, the liver weights and liver weights/body weights were assessed. The liver

weights were measured after sacrifice. The liver weights in grams in the HFD-SNP0 group were significantly increased compared to those of the ND-SNP0 group ( $p < 0.05$ , ANOVA) (Fig. 2a); this finding suggested that the HFD could cause increased liver dysfunction, which was similar to findings in previous research [2, 8, 42]. In

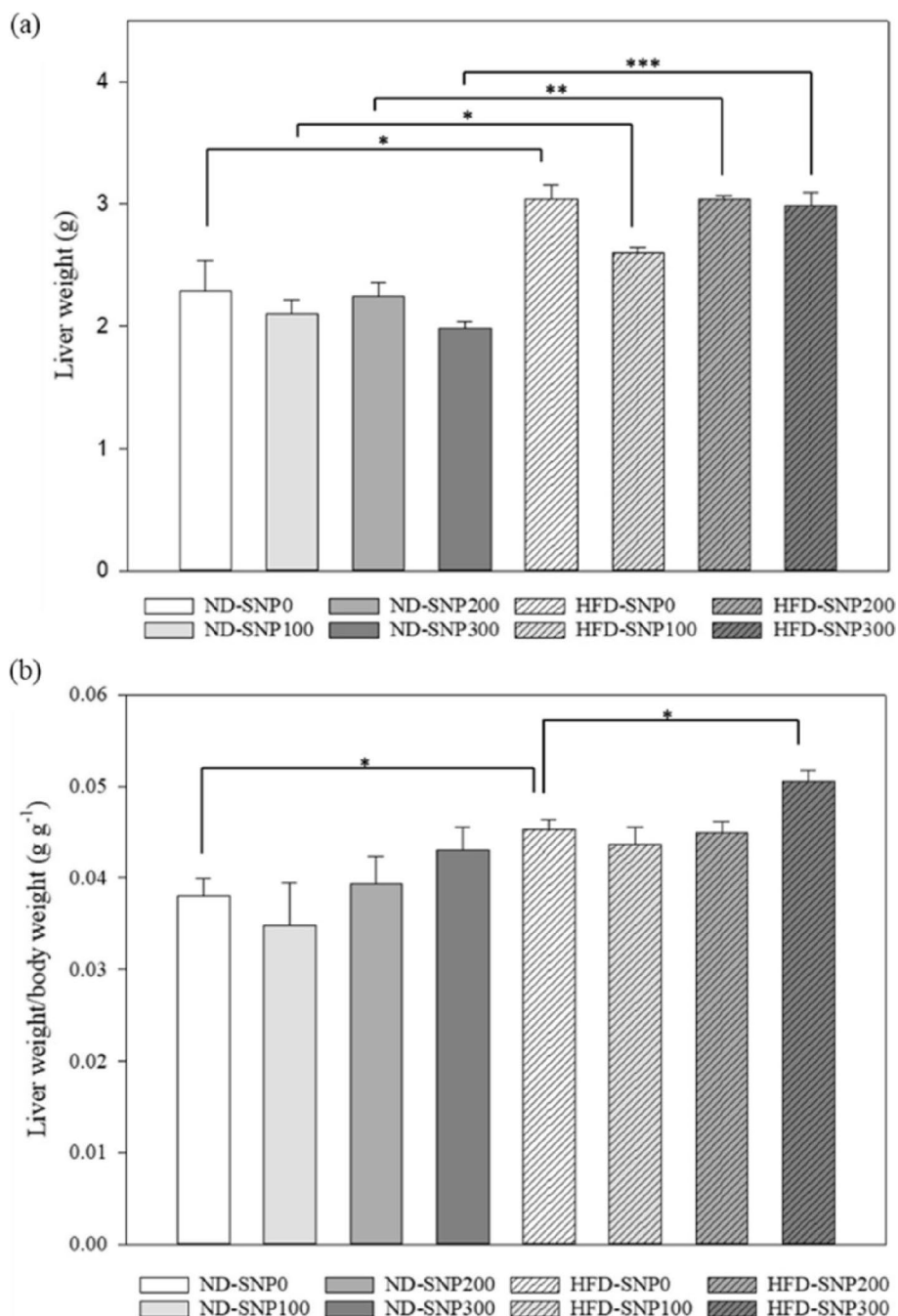


**Fig. 2** The average weight of the liver and liver weight per mouse body weight. The average weight of the liver in grams was measured at sacrifice after 25 weeks (a). The liver weight per mouse body weight (g g<sup>-1</sup>) was calculated after intragastric administration of SNPs for 25 consecutive weeks (twice per week) (b). Data are expressed as the means ± standard error of the means (n=6)

the ND treatment group, there was no significant liver weight difference in the ND-SNP0 group compared with the ND-SNP100, ND-SNP200, or ND-SNP300 groups ( $p > 0.05$ , ANOVA) (Fig. 2a). In each SNP treatment condition, the liver weights in the ND groups were lower than those in the HFD groups ( $p < 0.001$ – $0.05$ , ANOVA) (Fig. 2a). Figure 2b shows the liver weight/body weight (g liver weight/g mouse body weight). Liver weight/body weights were higher in the HFD-SNP0 group than in the ND-SNP0 group ( $p < 0.05$ , ANOVA); this evidence suggests that the HFD might induce liver dysfunction. There were no significant liver weight/body weight differences in the ND groups ( $p > 0.05$ , ANOVA) (Fig. 2b). In contrast, in the HFD-SNP300 groups, the liver weight/body weight was increased as compared with those of the HFD-SNP0 group ( $p < 0.05$ , ANOVA) (Fig. 2b), which indicated that injury might be caused in mice after long-term feeding with SNPs by oral gavage. Due to the silicon accumulation in liver tissue and liver weight/bodyweight results, liver dysfunction might be triggered by SNPs in HFD-fed mice.

#### 3.4 Induction of steatosis in the presence of SNPs in the HFD groups

To understand the microscopic organ structure and functions, H&E stains were used. In a healthy liver, hepatocytes express abundant clear cytoplasm due to the presence of glycogen [35, 43, 44]. The HFD-induced steatosis was apparent, which is based on the histopathological morphology and percentage of steatosis, in the HFD-SNP0 group compared with the ND-SNP0 group ( $p < 0.01$ , ANOVA) (Fig. 3a, b and i). In the ND-SNP100 and ND-SNP200 groups, H&E staining of hepatocytes showed an abundant clear cytoplasm, and no abnormal morphology transformations were seen in the mice compared with those in the ND-SNP0 group (Fig. 3a, c and e), suggesting the presence of normal hepatocytes in the ND-SNP100 and ND-SNP200 groups. Liver histopathological images illustrated that small numbers of clear fat-containing vacuoles and mild hepatic swelling could be seen in the mice of the ND-SNP300 group compared with those in the ND-SNP0 group (Fig. 3a and g), suggesting slight hepatocyte steatosis induced by SNPs. Previous studies with no or minor concern about SNPs found results similar to those in our ND groups subjected to SNP exposure [4, 36, 45]. Therefore, only SNPs may have no or minor influence on the liver, which is why  $\text{SiO}_2$  is used as a food additive. In the HFD groups, however, the livers of the mice treated with 100, 200, and 300  $\text{mg kg}^{-1}$  SNPs had enlarged hepatocytes, hepatocyte swelling, an increase in the degree of steatosis and the number of fat vacuoles, and a phenotype of deformed nuclei such as nuclear shrinkage and chromatin condensation,

compared to those in the HFD-SNP0 group (Fig. 3b, d, f and h), indicating overall liver degeneration. The percentage of steatosis (fat droplet area/total area) was analyzed by Image-Pro software and is shown in Fig. 3i. Based on the statistical results, the percentage of steatosis in the liver of mice in the ND-SNP300 group was significantly higher than that in the ND-SNP0 group, indicating an increase in steatosis due to SNPs ( $p < 0.05$ , ANOVA) (Fig. 3i). In the presence of administration of 200 or 300  $\text{mg kg}^{-1}$  SNPs in HFD group, the percentage of steatosis was increased compared to HFD-SNP0 group ( $p < 0.001$ , ANOVA), implying that liver steatosis was enhanced by SNPs in the HFD groups (Fig. 3i). Based on the statistical results, our evidence indicates that the injury might occur in mice after the intragastric administration of SNPs, which was confirmed by further experiments.

SNPs may pass through the cell membrane via endocytosis, including phagocytosis, pinocytosis, and receptor-mediated endocytosis, thereby damaging the plasma membrane and impairing the gut barrier [46]. In vitro binding assays have revealed that fatty acids and bovine serum albumin can interact with SNPs [47, 48]. Hence, the smaller the SNP diameter is for the same mass, the greater the surface area. A larger surface area increases the rates of interaction between SNPs and materials such as proteins, lipids, or other biohazardous chemicals and leads to a greater accumulation of the material through adsorption. Interestingly, other studies have shown that SNPs lead to reduced lipid absorption in vivo and in vitro [49, 50]. However, the correlation between SNPs and material adsorption and its underlying mechanisms are still unclear.

The percentage of fat droplets within the liver tissue indicates the level of liver steatosis. A healthy liver has less than 5% fat droplets in hepatocytes; mild fatty liver is indicated by 5–33% fat droplets in hepatocytes; moderate fatty liver is defined as 34–66% fat droplets in hepatocytes; and severe fatty liver contains more than 66% of fat droplets in hepatocytes [51, 52]. In our results, 0  $\text{mg kg}^{-1}$   $\text{SiO}_2$ -treated mice fed an ND showed normal liver morphology, but a combination of administration of 300  $\text{mg kg}^{-1}$  SNPs with an ND induced mild fatty liver, suggesting that SNPs might promote fatty liver formation. Similar results were found in the HFD groups; the HFD-SNP0, HFD-SNP100, and HFD-SNP200 groups showed mild fatty liver, and the HFD-SNP300 group showed moderate fatty liver. Therefore, NPs are a significant factor in fatty liver formation in mice fed an HFD.

The percentage of steatosis was increased in the SNP-treated groups of both the ND and HFD groups. However, the body weights did not change due to the SNP dose. Therefore, SNPs may have different effects in different tissues based on different underlying mechanisms.

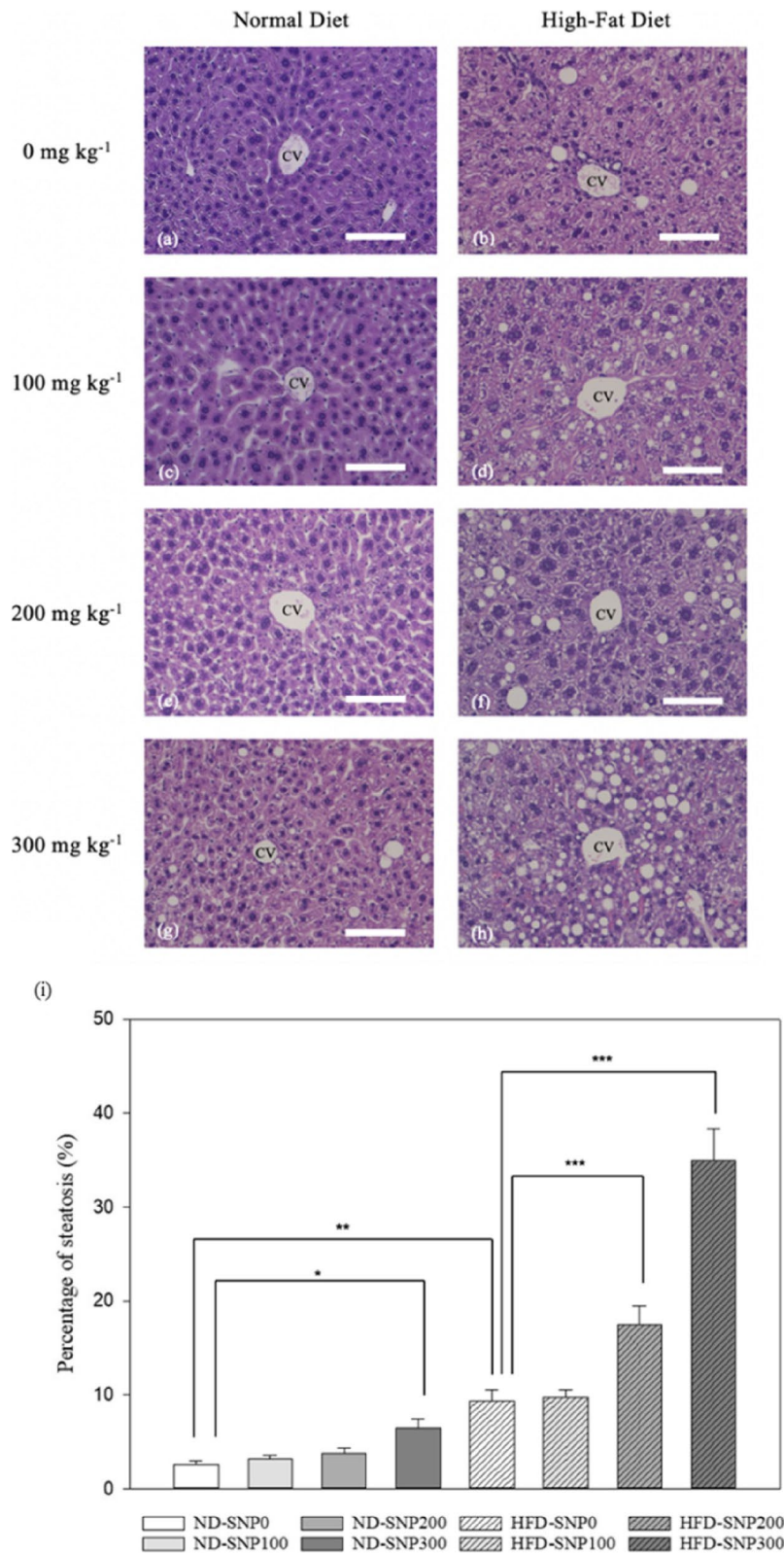


**Fig. 3** The degree of hepatic steatosis is shown by H&E staining. Mice were fed an ND (a, c, e, g) or an HFD (b, d, f, h) for 25 weeks. The mice were treated with 0 (a, b), 100 (c, d), 200 (e, f), and 300 (g, h) mg of SNPs kg<sup>-1</sup> mouse body weight twice per week. The central vein (CV) is indicated. Scale bars are 100 μm (a–h). Image-Pro software was used to analyze the percentage of steatosis area (steatosis area per total liver area) (i). Data are expressed as the means ± standard error of the means (n = 6)

Environmental nanoparticles, such as Titanium oxide and polystyrene NPs, have distinct chemical properties and actuate liver dysfunction, such as oxidative stress and apoptosis [53–56], duplicate our animal model. When particle size is in the nano level, many chemical and physical properties are changed, for example, semiconductor area. In summary, we suppose that NP size, not NP properties, may play a key role in induced liver dysfunction. To assess whether the effects of the different NPs in drinking water occur via similar mechanisms, more evidence is needed from further in vivo investigations.

### 3.5 Biochemical analyses in the serum of mice and TG level in mice liver

Our research analyzed levels of biochemical blood parameters, such as AST, ALT, T-CHO, TG, LDL, and HDL-C, in the serum of mice subjected to SNP administration to determine liver function in the mice. Biochemical analysis outcomes measured at 6, 12, and

25 weeks were compared, and no detectable differences were observed in T-CHO, TG, LDL, and HDL-C levels in either the ND or HFD SNP-administrated groups compared to their relative controls, which were only given reverse osmosis water ( $p > 0.05$ , ANOVA) (Table S1). The serum levels of AST and ALT were increased at 25 weeks in the HFD-SNP0 group compared with the ND-SNP0 group ( $p < 0.05$ , ANOVA) (Fig. 4a and b). AST and ALT levels were not changed at 25 weeks in the ND-SNP100 and ND-SNP200 groups compared to the ND-SNP0 group ( $p > 0.05$ , ANOVA) (Fig. 4a). However, an increase in AST level ( $p < 0.05$ , ANOVA), but no change in ALT level ( $p > 0.05$ , ANOVA), was found when in the ND-SNP300 group compared with the ND-SNP0 group (Fig. 4a). In the HFD-SNP200 and HFD-SNP300 groups, the levels of AST and ALT were significantly higher than those in the HFD-SNP0 group at 25 weeks ( $p < 0.001–0.05$ , ANOVA) (Fig. 4a and b).

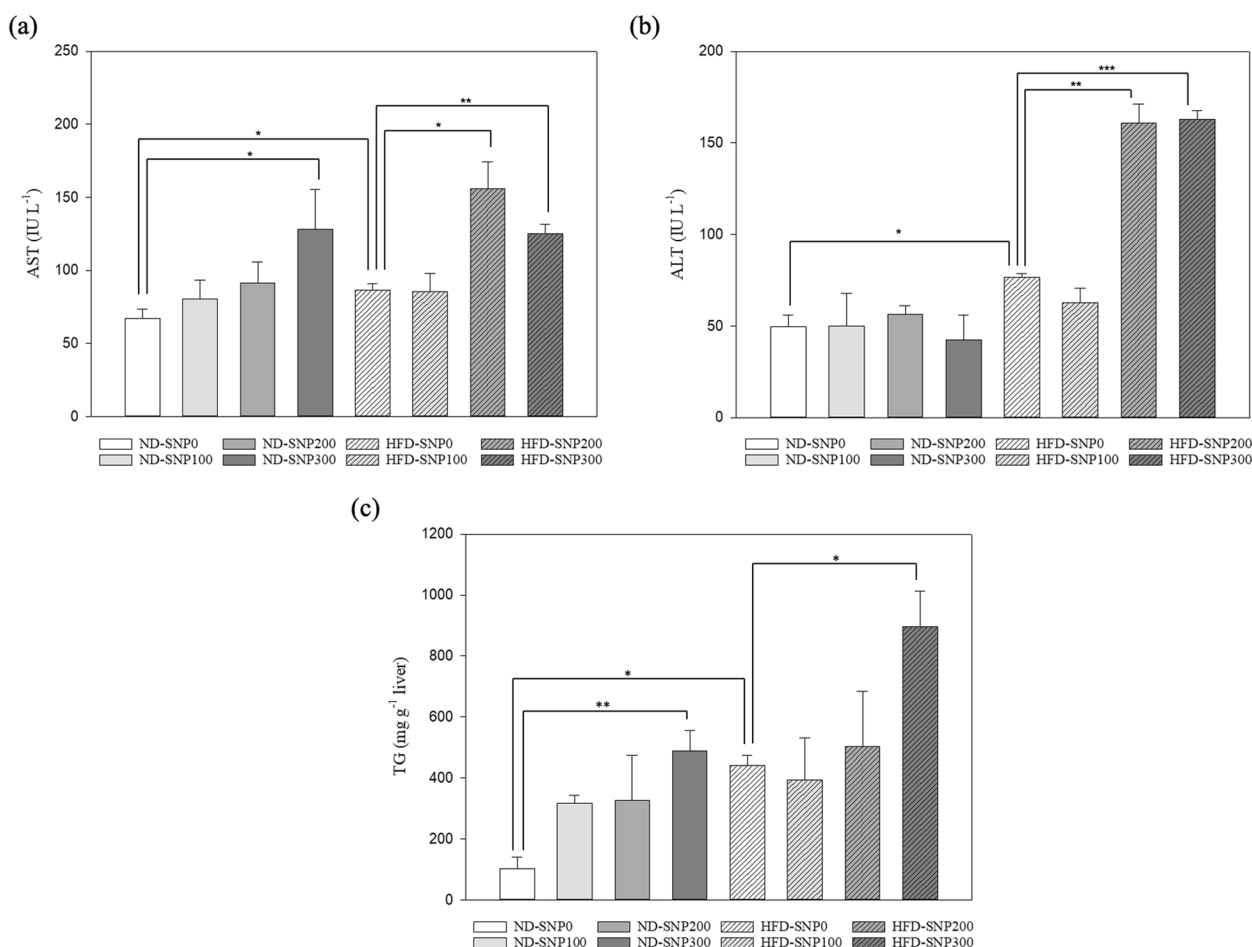


**Fig. 4** The expression of AST and ALT in serum and TG in liver tissue. Serum level of AST in IU L<sup>-1</sup> (a) and ALT in IU L<sup>-1</sup> (b) induced by SiO<sub>2</sub> nanoparticles in the ND and HFD groups at 25 weeks. The accumulation of liver TG content (mg of TGs g<sup>-1</sup> liver) in ICR mice was measured at 25 weeks (c). Data are expressed as the means ± standard error of the means (n = 6)

Lipid droplets are intracellular organelles specialized for the storage of energy in the form of neutral lipids such as TGs, the main content in lipid droplets. To further assess TG accumulation in liver tissue, a TG extraction method was performed in homogeneous liver tissue. TG accumulation was promoted by the HFD in the HFD-SNP0 group compared with the ND-SNP0 group ( $p < 0.05$ , ANOVA) (Fig. 4c). The accumulation of TGs, which is another confirmation of liver dysfunction, revealed that fatty liver was developed in the mice of the ND-SNP300 and HFD-SNP300 groups compared with those in the ND-SNP0 and HFD-SNP0 groups ( $p < 0.01$ – $0.05$ , ANOVA) (Fig. 4c). Further, the presence of SNPs in drinking water might have a deep influence over the long term and combined with HFD cause severely liver steatosis in our study.

The usual ranges of AST and ALT in ICR mice are 42–106 IU L<sup>-1</sup> and 28–59 IU L<sup>-1</sup>, respectively [57]. The amounts of AST and ALT in the serum were used to estimate the liver injury level and overweight/obesity, such as due to induction by NPs, fatty acid accumulation in the liver, viruses, and drugs [20, 25, 27, 31, 32, 58]. Under normal conditions, both enzymes are stored in the liver, and the contents of both enzymes in the blood are low. Therefore, the authors concluded that combining environmental NPs and high-fat food might stimulate aggravated liver damage formation. When the liver is seriously damaged by cirrhosis, only a high AST abnormality is often found [58]. Our results showed only a high serum level of AST in the ND-SNP300 group; more evidence is needed to prove this hypothesis, which SNPs could induce cirrhosis. In the HFD-fed mice, serum levels of biochemical parameters, including AST and ALT, and TGs in liver tissue were increased with long-term SNP treatment; therefore, SNP intake carries a potential risk and aggravates the impact of overweight/obesity and liver dysfunction in an HFD setting, which is representative of modern eating habits.

### 3.6 Liver steatosis characteristics in a mouse model

When fatty liver develops, nonalcoholic steatosis, which causes fat accumulation, occurs in liver cells. Hepatocyte swelling, inflammation, cell apoptosis, and fibrosis are observed during the progression of fatty liver formation [2, 3, 5–7].

#### 3.6.1 Induction of apoptosis

In fatty liver cells, apoptosis is considered a basic biological and physiological process. Its dysregulation is found in many pathologies and diseases, including damage through NP/common environmental pollutant toxicity, virus infection, immune cells, tumors, and metabolism [59, 60]. It is characterized by the presence

of concentrated chromatin and DNA breakage. TUNEL staining is a classical method for the detection of DNA breakage and analyzing the percentage of apoptosis. TUNEL-positive cells were observed in the HFD-SNP200 and HFD-SNP300 groups of mice (Fig. 5f and h). Quantitation of TUNEL-positive cells demonstrated a significant increase in apoptosis in the HFD-SNP200 and HFD-SNP300 groups of mice when compared with the HFD-SNP0 group ( $p < 0.05$ – $0.001$ , ANOVA) (Fig. 5i). These data show evidence that hepatocyte apoptosis can be induced by SNPs in modern dietary habits.

Cells such as those derived from the human liver (Hep G2), human kidney (HK-2 and HL-7702), human keratinocyte (HaCaT), human astrocytoma (U87), human epithelial (HeLa), human bone marrow (SH-SY5Y), and human lung (A549) treated with SNPs exhibit lipid peroxidation, oxidative stress, DNA repair, apoptosis, and cell cycle progression [22, 28, 61–64]. The mRNA and protein expression levels of the cell cycle checkpoint gene p53 and of apoptotic genes such as Bax and caspase-3 were upregulated, while the expression of the antiapoptotic gene Bcl-2 was downregulated [22, 61]. The expression levels of the cell signaling protein proteins ERK, p-ERK, NADH dehydrogenase subunit six, and mitochondrial DNA-encoded cytochrome C oxidase subunit II were altered [63]. These previous studies demonstrated that the SNP effect was highly related to apoptosis and was consistent with our experiment results. Previous studies reported that besides causing DNA damage, global genomic hypomethylation was induced by SNPs [65–67]. DNA damage could make the cell apoptosis already known. Epigenetic dysregulation may have long-term effects on gene expression and lead to long-term untoward effects in our mice model. However, the detailed mechanism of apoptosis through epigenetic dysregulation induced by SNPs is still unclear.

#### 3.6.2 Induction of fibrosis

Long-term steatosis leads to liver fibrosis buildup and the replacement of healthy liver tissue. The liver tissue also loses function since the healthy liver cells are lost. Without therapy or changing eating behavior, fatty liver will develop into cirrhosis or liver cancer [5, 6, 21]. Picrosirius red staining and Masson's trichrome staining were used to examine the liver fibrosis level in this study. In images of tissue stained with picrosirius red, no obvious fibrosis was observed in the ND diet groups that underwent treatment with SNPs compared with the ND-SNP0 group (Fig. 6a, c, e and g), and induction of fibrosis was observed in the HFD-SNP200 and HFD-SNP300 groups compared with the HFD-SNP0 group ( $p < 0.001$ – $0.01$ , ANOVA; Fig. 6b, f, h and i). Similarly, in images of tissue stained with Masson's trichrome, induction of

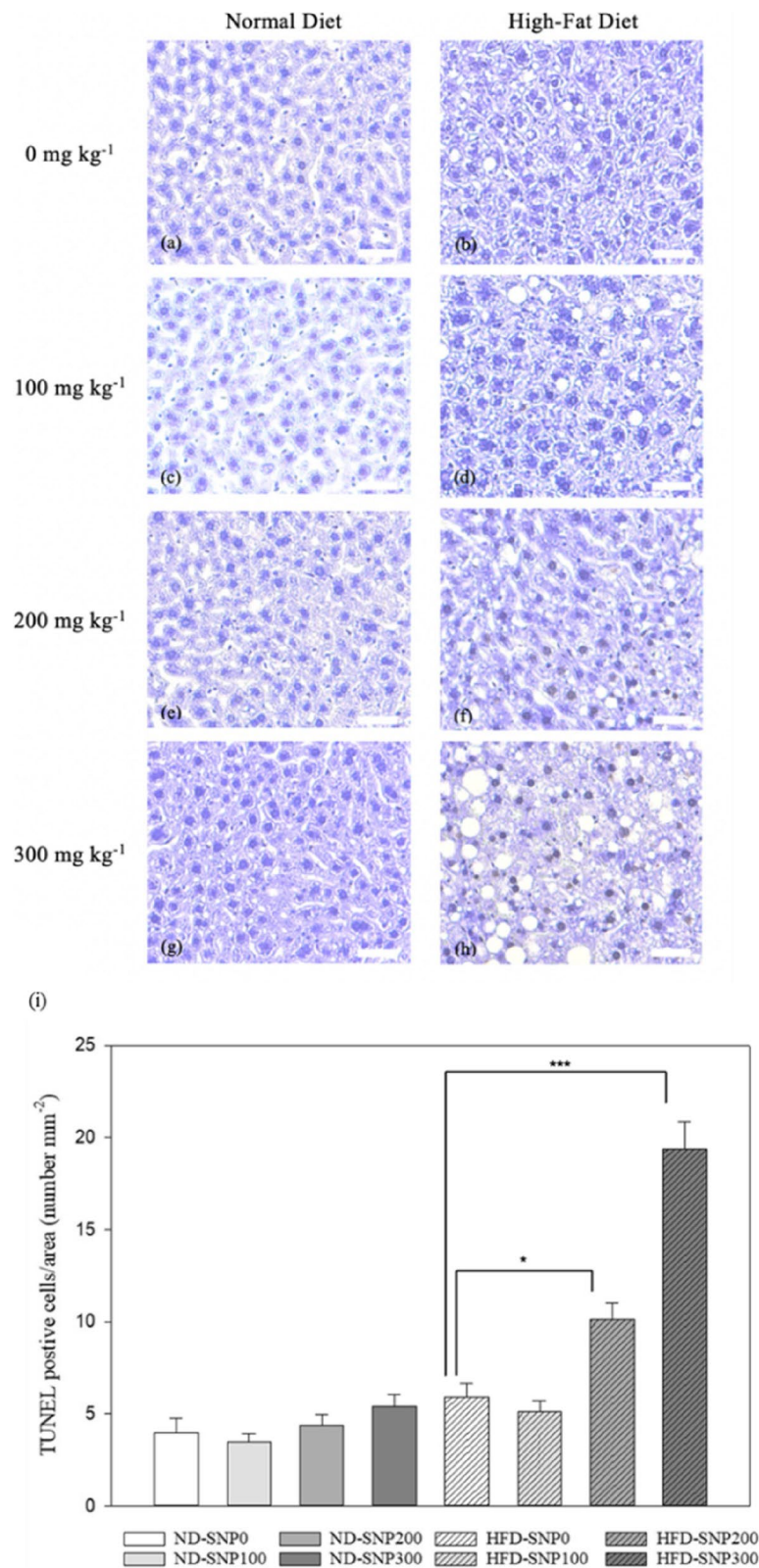


**Fig. 5** The degree of apoptosis is shown by TUNEL staining. Mice were fed the ND (a, c, e, g) or HFD (b, d, f, h) for 25 weeks. The mice were treated with 0 (a, b), 100 (c, d), 200 (e, f), and 300 (g, h) mg of SNPs kg<sup>-1</sup> mouse body weight twice per week. The CV is indicated. Scale bars are 50 μm (a–h). The quantification of TUNEL-positive cells was analyzed by Image-Pro (i). Data are expressed as the means ± standard error of the means (n = 6)

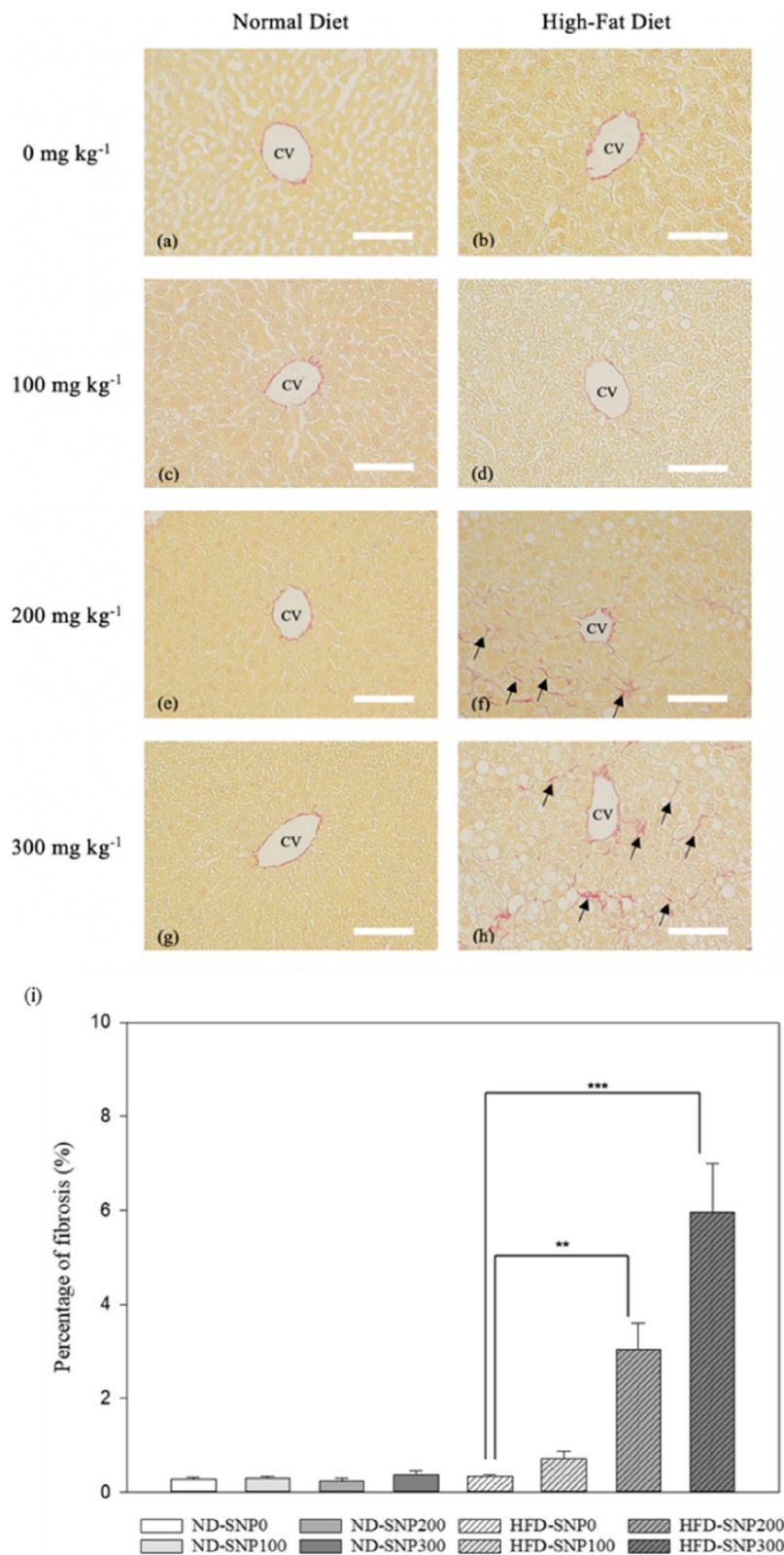


**Fig. 6** The degree of fibrosis is shown by picosirius red staining. Mice were fed the ND (a, c, e, g) or HFD (b, d, f, h) for 25 weeks. The mice were treated with 0 (a, b), 100 (c, d), 200 (e, f), and 300 (g, h) mg of SNPs kg<sup>-1</sup> mouse body weight twice per week. The arrow indicates positive picosirius red staining. The CV is indicated. Scale bars are 100 μm (a-h). The quantitative fibrosis was analyzed by Image-Pro (i). Data are expressed as the means ± standard error of the means (n = 6)

fibrosis caused by SNPs was found in the HFD-SNP200 and HFD-SNP300 groups compared with the HFD-SNP0 group ( $p < 0.001$ , ANOVA) (Figs. S2b, S2f, S2h and S2i). Controlling peroxisome proliferator-activated receptor (PPAR) $\alpha/\delta$ , Galectin-3, apoptosis signal-regulating kinase 1, and PPAR $\gamma$  were the possible mechanisms for liver fibrosis [68–71]. Some studies have shown that NPs can downregulate PPAR $\gamma$  and promote fibrosis [72]. The liver fibrosis seen in our mouse model may be caused by decreased PPAR $\gamma$  expression in liver tissue, but the author can not rule out another possibility.

### 3.6.3 Induction of inflammation

C-reactive protein (CRP) is a factor in predicting inflammation in the mouse model. When liver injury, infection, or other diseases occur, CRP levels increase and cause inflammation. CRP level did not change in our animal model (data not shown). Because no evident bodily damage was found in our animal model, no acute inflammation, an immediate, adaptive response to bodily damage such as a bite or a cut, could be found. Hence, chronic inflammation, considered to be slow, long-term inflammation over several months to years, is another potential possibility. To understand chronic inflammation caused by SNPs, CD3 is expressed in the cell membrane and cytoplasm and is usually found in cytotoxic T and T helper cells. The number of CD3<sup>+</sup> immune cells was increased in the ND-SNP-300, HFD-SNP200, or HFD-SNP300 groups compared to the ND-SNP0 or HFD-SNP0 groups ( $p < 0.05$ – $0.001$ , ANOVA) (Fig. 7a, b, f, g, h and i).

Liver dysfunction could lead to the accumulation of inflammatory cells in liver tissue, causing liver damage and the secretion of proinflammatory cytokines, including TNF- $\alpha$  and IL-6 [73]. To determine the level of inflammation, IHC was used to detect the secretion of TNF- $\alpha$  and IL-6. IL-6 expression in the HFD-SNP200 and HFD-SNP300 groups was increased compared to that in the HFD-SNP0 group ( $p < 0.01$ – $0.001$ , ANOVA) (Figs. S3f, S3h and S3i). However, TNF- $\alpha$  expression was not distinct in our model (Fig. S4). Based on the increased CD3<sup>+</sup> cells and secretion of IL-6, inflammation is thought to be induced in our model.

### 3.6.4 Increased oxidative stress by 4-HNE staining

Oxidative stress caused by NP injury is a common feature in chronic liver disease [9, 74]. The 4-HNE protein expression in the cytoplasm is a marker of oxidative stress [75] and can inhibit the expression of PPAR $\gamma$  and enhance oxidative stress levels [76]. The 4-HNE level in liver tissue was shown by IHC staining. The results showed a reinforced 4-HNE-positive area in mice fed 300 mg of SNP kg<sup>-1</sup> mouse body weight in the HFD

group compared with 0 mg of SNP kg<sup>-1</sup> mouse body weight in the HFD group (Fig. 8b and h). In Fig. 8i, the quantitative data analyzed by Image-Pro showed that the percentage of the 4-HNE-positive area was increased to 3.9% when the HFD-SNP300 group was compared to the HFD-SNP0 group ( $p < 0.05$ , ANOVA), showing that hepatic oxidative stress was exacerbated in the HFD-SNP300 group.

Increasing amounts of evidence suggest that the development of liver steatosis is related to environmental factors, especially the enormous influence of NPs exposure [53–56]. The liver is commonly regarded as the accumulative organ for NP absorption. Previous research has revealed that SNP exposure can cause liver injury, steatosis, fibrosis, inflammation, and apoptosis [17, 19, 21–26]. In the pathophysiology of fatty liver disease, accumulated TG is thought to exceed and affect the oxidative catabolism of free fatty acids [77]. Indeed, our data reveal that SNP exposure combined with HFD facilitated the aggravated development of liver steatosis using in vivo investigations. In the HFD group mice fed SNPs, the chronic exposure to SNPs promoted fatty liver in the liver and the levels of AST and ALT in the serum and the histopathological analysis. Consistently, TG accumulation, fibrosis, inflammation, apoptosis, and oxidative stress were also enhanced in HFD-treated mice fed SNPs.

Recently, metabolomics has been applied to metabolic disorder analysis and analysis of biomarkers in different disease states [78]. Perturbed metabolism, such as that of amino acids, lipids, and glucose, is crucial to the development of fatty liver disease [79]. The amount of AST and ALT in serum may be sensors of global metabolic dysregulation. In the abnormal accumulation of TG in the liver, elevated aminotransferases are a marker for liver metabolic disorder. Other explorations related to liver metabolism have shown that raising AST and ALT levels may not come from liver damage. The elevated AST and ALT levels may be the consequence of unusual amino acid and energy metabolism in the liver [80]. Certainly, an in-depth exploration of the observed metabolites is particularly important to fully elucidate the effect of SNPs on aggravated liver injury in modern dietary habits.

As drinking water is rich in NPs, increasing levels of NPs may, due to the increased serum levels of AST and ALT, possibly lead to liver injury. Interestingly, our research found increased AST but not ALT in ND-treated mice fed SNPs. AST is expressed not only in the liver but also in other organs, such as the skeletal muscles and heart [81]. One of the most common non-hepatic causes of elevated AST levels is skeletal muscle damage (rhabdomyolysis) [82]. In cardiovascular disease patients, increased serum AST is routinely used for the diagnosis of acute myocardial infarction [83]. In our animal model,

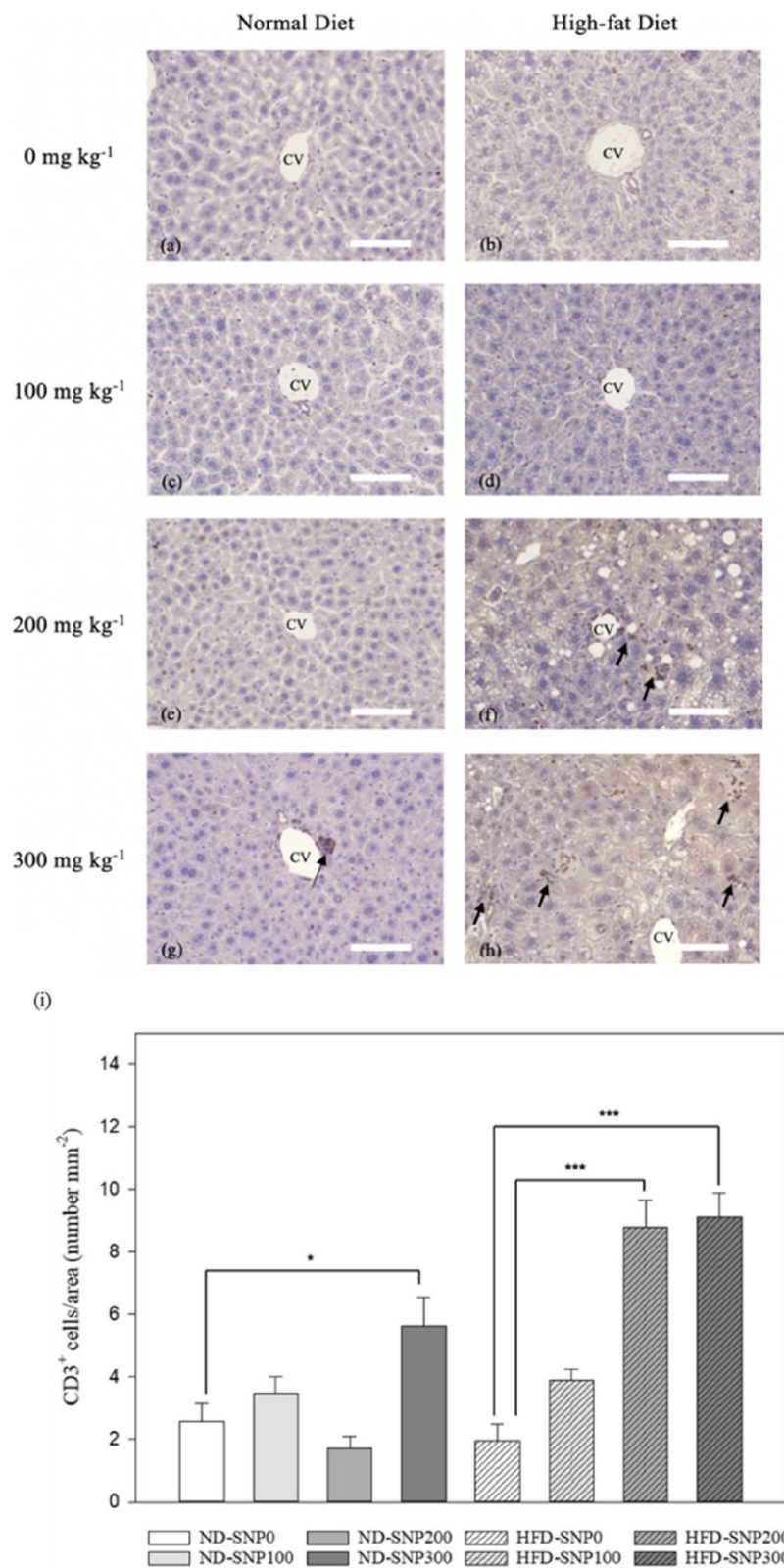


**Fig. 7** The proportion of CD3<sup>+</sup> cells is shown by immunohistochemistry stain. Mice were fed the ND (a, c, e, g) or HFD (b, d, f, h) for 25 weeks. The mice were treated with 0 (a, b), 100 (c, d), 200 (e, f), and 300 (g, h) mg of SNPs kg<sup>-1</sup> mouse body weight twice per week. The arrow indicates immune cells with the CD3 marker. The CV is indicated. Scale bars are 100 μm (a–h). The quantity of CD3<sup>+</sup> cells was analyzed by Image-Pro (i). Data are expressed as the means ± standard error of the means (n=6)

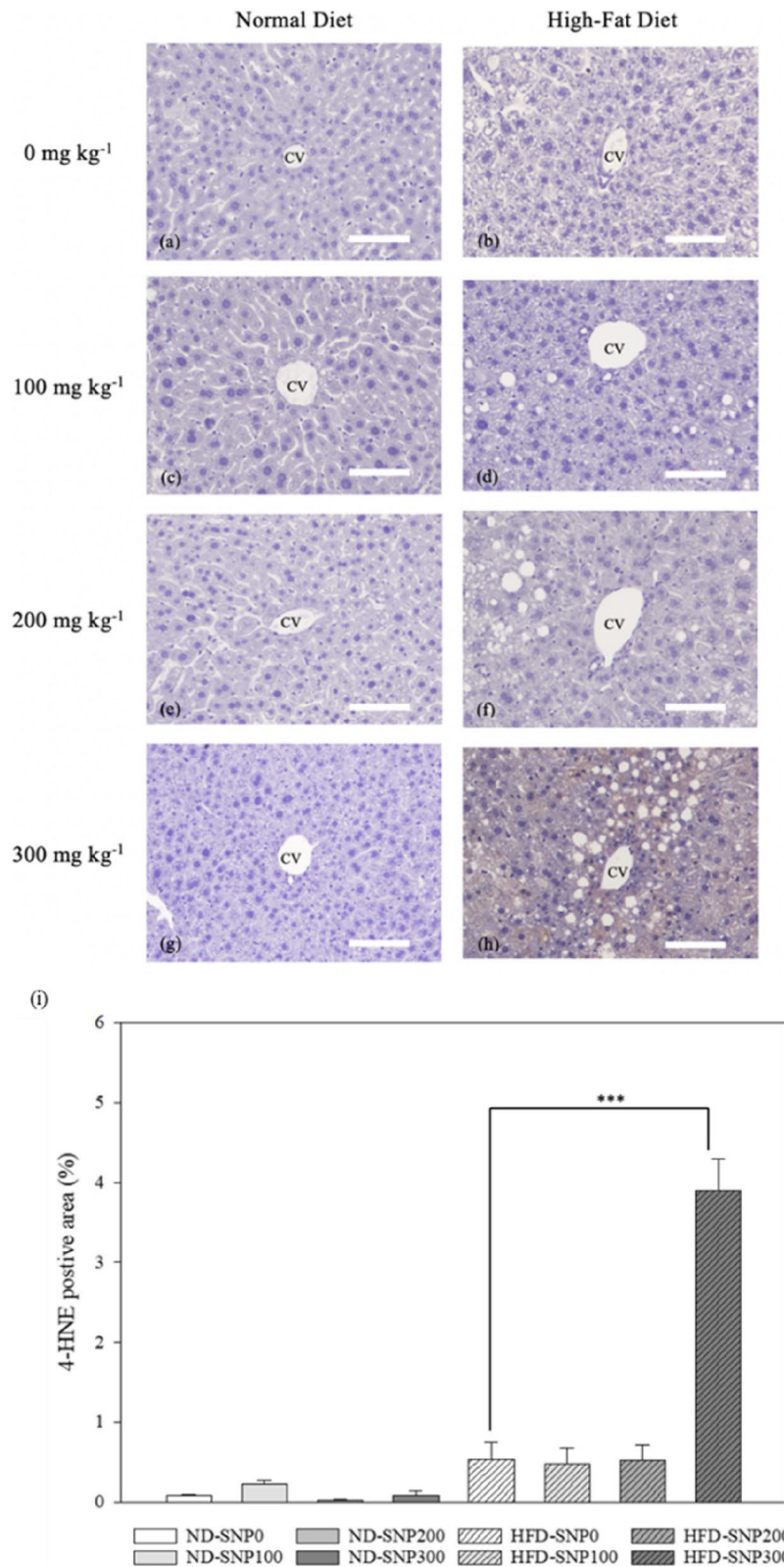


**Fig. 8** The degree of oxidative stress is shown by staining for 4-HNE using immunohistochemistry. Mice were fed the ND (a, c, e, g) or HFD (b, d, f, h) for 25 weeks. The mice were treated with 0 (a, b), 100 (c, d), 200 (e, f), and 300 (g, h) mg of SNPs kg<sup>-1</sup> mouse body weight twice per week. The CV is indicated. Scale bars are 100 μm (a–h). The percentage of positive 4-HNE staining/area was analyzed by Image-Pro (i). Data are expressed as the means ± standard error of the means (n = 6)

SNPs might induce serum AST at 25 weeks, and injury may occur not only in the liver but also in other organs.

Inflammatory cytokines play significant roles in the progression of liver steatosis. For instance, SNPs promoted the expression of IL-6 and TNF- $\alpha$  in cell lines or patients with nonalcoholic steatohepatitis [20]. The TNF- $\alpha$  and IL-6 may play a key role in lipid metabolism [84, 85]. In our animal model, IL-6 levels, rather than those of TNF- $\alpha$ , were increased. Therefore, IL-6 is crucial for hepatocyte homeostasis and is implicated in metabolic function in the liver.

The stability of SNPs has been inconsistent [86, 87]. When SNPs interact with the biological medium, the stability of the SNP structure and the interaction between SNPs and media may determine the activity of nanomaterials in vivo. Silicosis, a type of progressive, irreversible, and fatal lung inflammation and fibrosis, is a lung disease caused by inhaling silicon dioxide. Even after exposure to silica, the silica NPs remain in the lungs and continually damage the lungs toward the development of chronic silicosis. This evidence suggests that SNPs are stable and cannot easily break down in the body. To date, the half-life of SNPs and breakdown metabolism in the liver is still poorly understood. Clarifying the half-life mechanism of SNPs will help to understand the role of SNPs in liver steatosis.

PPAR $\alpha$ , highly expressed in normal mouse and human livers, activates transcription and represses lipid accumulation [88, 89]. Some studies have shown that NPs can inhibit PPAR $\alpha$  in the liver [90]. Yu et al. have demonstrated that PPAR $\alpha$  and target genes for PPAR $\alpha$ , such as Acyl-CoA dehydrogenase, lipoprotein lipase, and Acyl-CoA oxidase 1, inhibit lipid accumulation and liver steatosis [91]. Therefore, the potential mechanism of liver steatosis in a combination of SNPs and a high-fat diet mice model may be decreased PPAR $\alpha$  and target genes for PPAR $\alpha$ .

Although a recent study explained how an HFD promotes steatosis, the correlation between the SNPs and the HFD was not reported. This study further corroborates our assumption that SNPs induce fat accumulation in hepatic cells and induce steatosis through oxidative stress in HFD-fed mice.

#### 4 Conclusions

An animal study was carried out using SNPs, which were used to imitate the NPs found in drinking water, either a normal or high-fat diet, in a mouse model. Body weights, liver weights, histology of the livers, blood biochemistry assays, fibrosis staining, TUNEL staining, and immunohistochemical staining were used to characterize the effect of the administration of different SNP concentrations (100–300 mg of SNP kg<sup>-1</sup> mouse body weight) over

25 weeks. The results showed that animal weights did not change in either the ND or HFD groups fed different concentrations of SNPs. No abnormal clinical signs or animal behaviors were found in our animal model. An increase in the liver weight to body weight ratio and an accumulation of silicon were observed and might be closely related to liver degeneration in the presence of the combination of SNPs and an HFD. Biochemical blood assays revealed that T-CHO, TG, HDL-C, and LDL levels were not significantly altered in our model. However, the enhanced steatosis, analyzed by H&E morphology staining, and TG accumulation in liver tissue showed that liver function was affected. The increased ALT and AST levels also confirmed that liver damage was induced in mice fed SNPs in the HFD groups. Induced fibrosis and inflammation were also observed in mice fed SNPs in the HFD groups. Upregulated oxidative stress was identified by 4-HNE IHC. Considering the results of our study, SNPs in drinking water may represent a hazard to liver function in the setting of modern dietary habits.

A modern dietary pattern, such as the consumption of high-fat food, is becoming more common. SNPs already exist in drinking water and are used in numerous applications, such as food additives and drug delivery. In our mouse model, induced liver steatosis was observed. Hence, our outcome demonstrates a correlation between SNPs and modern dietary patterns. The detailed mechanism of induced liver steatosis and its signal transduction by SNPs and HFD remains unclear; nevertheless, the induction of oxidative stress was determined in our model. Although outbred mice showed the relationship between SNPs and modern dietary patterns, the mouse model still differs from humans. To understand the effects of SNPs on the human body, more experiments, such as long-term monitoring of the accumulation of SNPs in the environment and human body, are necessary. Based on our conclusion, we cannot ignore the influence of SNPs on the rise in our daily lives. The research provides valuable insights into environmental nanoparticles and dietary factors, suggesting essential risks to liver health.

#### Supplementary Information

The online version contains supplementary material available at <https://doi.org/10.1186/s42834-024-00237-7>.

Supplementary Material 1.

#### Acknowledgements

We thank the Taiwan Mouse Clinic, Academia Sinica, and Taiwan Animal Consortium for technical support in mouse sacrifice, H&E staining, blood biochemistry assays, and immunohistochemistry.

### Authors' contributions

Tzung Cheng Ye: Conceptualization, writing - original draft, investigation, visualization. Shu-Ju Chao: Conceptualization. Ru-Tsun Mai: Conceptualization. Chihpin Huang: Conceptualization, supervision, resources. All authors have read and agreed to the published version of the manuscript.

### Funding

Funding agency: Ministry of Science and Technology Taiwan. Grant number: MOST 108-2221-E-009-074-MY3. Animal study ethics approval from National Yang Ming Chao Tung University (National Chao Tung University). Approval number: NCTU-IACUC-107052.

### Data availability

The data that supports the findings of this study are available within the article.

### Declarations

#### Competing interests

The authors declare they have no competing interests.

Received: 15 April 2024 Accepted: 2 December 2024

Published online: 18 December 2024

### References

- Romieu I, Dossus L, Barquera S, Blottiere HM, Franks PW, Gunter M, et al. Energy balance and obesity: what are the main drivers? *Cancer Cause Control*. 2017;28:247–58.
- Nagaoka K, Mulla J, Cao K, Cheng Z, Liu D, William M, et al. The metabolite, alpha-ketoglutarate inhibits non-alcoholic fatty liver disease progression by targeting lipid metabolism. *Liver Res*. 2020;4:94–100.
- Heeren J, Scheja L. Metabolic-associated fatty liver disease and lipoprotein metabolism. *Molecular Metabolism*. 2021;50:101238.
- Yu Y, Li Y, Wang W, Jin M, Du Z, Li Y, et al. Acute toxicity of amorphous silica nanoparticles in intravenously exposed ICR mice. *PLoS One*. 2013;8:e61346.
- Heyens LJM, Busschots D, Koek GH, Robaey G, Francque S. Liver fibrosis in non-alcoholic fatty liver disease: from liver biopsy to non-invasive biomarkers in diagnosis and treatment. *Front Med*. 2021;8:615978.
- Peng C, Stewart AG, Woodman OL, Ritchie RH, Qin CX. Non-alcoholic steatohepatitis: a review of its mechanism, models, and medical treatments. *Front Pharmacol*. 2020;11:603926.
- Liang Q, Sun M, Ma Y, Wang F, Sun Z, Duan J. Adverse effects and underlying mechanism of amorphous silica nanoparticles in liver. *Chemosphere*. 2023;311:136955.
- VanSaun MN, Lee IK, Washington MK, Matrisian L, Gorden DL. High fat diet induced hepatic steatosis establishes a permissive microenvironment for colorectal metastases and promotes primary dysplasia in a murine model. *Am J Pathol*. 2009;175:355–64.
- Airanthi MKWA, Sasaki N, Iwasaki S, Baba N, Abe M, Hosokawa M, et al. Effect of brown seaweed lipids on fatty acid composition and lipid hydroperoxide levels of mouse liver. *J Agr Food Chem*. 2011;59:4156–63.
- Dohi K, Kraemer BC, Erickson MA, McMillan PJ, Kovac A, Flachbartova Z, et al. Molecular hydrogen in drinking water protects against neurodegenerative changes induced by traumatic brain injury. *PLoS One*. 2014;9:e108034.
- Chao SJ, Huang CP, Lam CC, Hua LC, Chang SH, Huang C. Transformation of copper oxide nanoparticles as affected by ionic strength and its effects on the toxicity and bioaccumulation of copper in zebrafish embryo. *Ecotox Environ Safe*. 2021;225:112759.
- Sousa VS, Ribau Teixeira M. Metal-based engineered nanoparticles in the drinking water treatment systems: A critical review. *Sci Total Environ*. 2020;707:136077.
- Chang HH, Cheng TJ, Huang CP, Wang GS. Characterization of titanium dioxide nanoparticle removal in simulated drinking water treatment processes. *Sci Total Environ*. 2017;601–602:886–94.
- Yang Y, Faust JJ, Schoepf J, Hristovski K, Capco DG, Herckes P, et al. Survey of food-grade silica dioxide nanomaterial occurrence, characterization, human gut impacts and fate across its lifecycle. *Sci Total Environ*. 2016;565:902–12.
- EFSA ANS Panel, Younes M, Aggett P, Aguilar F, Crebelli R, Dusemund B, et al. Re-evaluation of silicon dioxide (E 551) as a food additive. *EFSA J*. 2018;16:5088.
- Khan I, Saeed K, Khan I. Nanoparticles: Properties, applications and toxicities. *Arab J Chem*. 2019;12:908–31.
- Zhu Y, Zhang Y, Li Y, Guo C, Fan Z, Li Y, et al. Integrative proteomics and metabolomics approach to elucidate metabolic dysfunction induced by silica nanoparticles in hepatocytes. *J Hazard Mater*. 2022;434:128820.
- Sasai F, Rogers KL, Orlicky DJ, Stem A, Schaeffer J, Garcia G, et al. Inhaled silica nanoparticles cause chronic kidney disease in rats. *Am J Physiol Renal*. 2022;323:F48–58.
- Li X, Li Y, Lv S, Xu H, Ma R, Sun Z, et al. Long-term respiratory exposure to amorphous silica nanoparticles promoted systemic inflammation and progression of fibrosis in a susceptible mouse model. *Chemosphere*. 2022;300:134633.
- Abulikemu A, Zhao X, Xu H, Li Y, Ma R, Yao Q, et al. Silica nanoparticles aggravated the metabolic associated fatty liver disease through disturbed amino acid and lipid metabolisms-mediated oxidative stress. *Redox Biology*. 2023;59:102569.
- Yu Y, Duan J, Li Y, Li Y, Jing L, Yang M, et al. Silica nanoparticles induce liver fibrosis via TGF- $\beta_1$ /Smad3 pathway in ICR mice. *Int J Nanomedicine*. 2017;12:6045–57.
- Zuo D, Duan Z, Jia Y, Chu T, He Q, Yuan J, et al. Amphipathic silica nanoparticles induce cytotoxicity through oxidative stress mediated and p53 dependent apoptosis pathway in human liver cell line HL-7702 and rat liver cell line BRL-3A. *Colloid Surfaces B*. 2016;145:232–40.
- He H, Zhou Y, Liu L, Cui J, Pei Y, Cao J, et al. Bioinformatics analysis reveals lipid metabolism may play an important role in the SiO<sub>2</sub>-stimulated rat model. *Cell Signal*. 2023;108:110716.
- Yang X, Liu J, He H, Zhou L, Gong C, Wang X, et al. SiO<sub>2</sub> nanoparticles induce cytotoxicity and protein expression alteration in HaCaT cells. *Part Fibre Toxicol*. 2010;7:1.
- Almansour M, Alarifi S, Jarrar B. In vivo investigation on the chronic hepatotoxicity induced by intraperitoneal administration of 10-nm silicon dioxide nanoparticles. *Int J Nanomedicine*. 2018;13:2685–96.
- Guilloteau E, Djouina M, Caboche S, Waxin C, Deboudt K, Beury D, et al. Exposure to atmospheric Ag, TiO<sub>2</sub>, Ti and SiO<sub>2</sub> engineered nanoparticles modulates gut inflammatory response and microbiota in mice. *Ecotox Environ Safe*. 2022;236:113442.
- Hassankhani R, Esmaeilou M, Tehrani AA, Nasirzadeh K, Khadir F, Maadi H. In vivo toxicity of orally administered silicon dioxide nanoparticles in healthy adult mice. *Environ Sci Pollut R*. 2015;22:1127–32.
- Roshanfekrnahzomi Z, Badpa P, Esfandiari B, Taheri S, Nouri M, Akhtari K, et al. Silica nanoparticles induce conformational changes of tau protein and oxidative stress and apoptosis in neuroblastoma cell line. *Int J Biol Macromol*. 2019;124:1312–20.
- Deciga-Alcaraz A, Medina-Reyes EI, Delgado-Buenrostro NL, Rodriguez-Ibarra C, Ganem-Rondero A, Vazquez-Zapien GJ, et al. Toxicity of engineered nanomaterials with different physicochemical properties and the role of protein corona on cellular uptake and intrinsic ROS production. *Toxicology*. 2020;442:152545.
- Cheng Y, Chen Z, Yang S, Liu T, Yin L, Pu Y, et al. Nanomaterials-induced toxicity on cardiac myocytes and tissues, and emerging toxicity assessment techniques. *Sci Total Environ*. 2021;800:149584.
- Li Z, He J, Li B, Zhang J, He K, Duan X, et al. Titanium dioxide nanoparticles induce endoplasmic reticulum stress-mediated apoptotic cell death in liver cancer cells. *J Int Med Res*. 2020;48:0300060520903652.
- Wang J, Zhou G, Chen C, Yu H, Wang T, Ma Y, et al. Acute toxicity and biodistribution of different sized titanium dioxide particles in mice after oral administration. *Toxicol Lett*. 2007;168:176–85.
- Lee SY, Kim IY, Heo MB, Moon JH, Son JG, Lee TG. Global proteomics to study silica nanoparticle-induced cytotoxicity and its mechanisms in HepG2 cells. *Biomolecules*. 2021;11:375.
- Chan WT, Liu CC, Chiang Chia JS, Tsai ST, Liang CK, Cheng ML, et al. In vivo toxicologic study of larger silica nanoparticles in mice. *Int J Nanomedicine*. 2017;12:3421–32.

35. Murugadoss S, Lison D, Godderis L, Van Den Brule S, Mast J, Brassinne F, et al. Toxicology of silica nanoparticles: an update. *Arch Toxicol*. 2017;91:2967–3010.
36. Cabellos J, Gimeno-Benito I, Catalan J, Lindberg HK, Vales G, Fernandez-Rosas E, et al. Short-term oral administration of non-porous and mesoporous silica did not induce local or systemic toxicity in mice. *Nanotoxicology*. 2020;14:1324–41.
37. Koronowski KB, Kinouchi K, Welz PS, Smith JG, Zinna VM, Shi J, et al. Defining the Independence of the Liver Circadian Clock. *Cell*. 2019;177:1448–62.
38. Stokkan KA, Yamazaki S, Tei H, Sakaki Y, Menaker M. Entrainment of the circadian clock in the liver by feeding. *Science*. 2001;291:490–3.
39. March S, Nerurkar N, Jain A, Andrus L, Kim D, Whittaker CA, et al. Autonomous circadian rhythms in the human hepatocyte regulate hepatic drug metabolism and inflammatory responses. *Sci Adv*. 2024;10:eadm9281.
40. Peters RJB, Oomen AG, van Bommel G, van Vliet L, Undas AK, Munniks S, et al. Silicon dioxide and titanium dioxide particles found in human tissues. *Nanotoxicology*. 2020;14:420–32.
41. Jones LHP, Handreck KA. Silica In Soils, Plants, and Animals. In: Norman AG, editor. *Adv Agron*. 1967;19:107–49.
42. Kirpich IA, Gobejishvili LN, Homme MB, Waigel S, Cave M, Arteel G, et al. Integrated hepatic transcriptome and proteome analysis of mice with high-fat diet-induced nonalcoholic fatty liver disease. *J Nutr Biochem*. 2011;22:38–45.
43. Soon GST, Torbenson M. The liver and glycogen: in sickness and in health. *Int J Mol Sci*. 2023;24:6133.
44. Kim JH, Kim CS, Ignacio RM, Kim DH, Sajo ME, Maeng EH, et al. Immunotoxicity of silicon dioxide nanoparticles with different sizes and electrostatic charge. *Int J Nanomedicine*. 2014;9:183–93.
45. Boudard D, Aureli F, Laurent B, Sturm N, Raggi A, Antier E, et al. Chronic oral exposure to synthetic amorphous silica (NM-200) results in renal and liver lesions in mice. *Kidney International Reports*. 2019;4:1463–71.
46. Yong CQY, Vallyaveettil S, Tang BL. Toxicity of microplastics and nanoplastics in mammalian systems. *Int J Env Res Pub He*. 2020;17:1509.
47. Givens BE, Diklich ND, Fiegel J, Grassian VH. Adsorption of bovine serum albumin on silicon dioxide nanoparticles: Impact of pH on nanoparticle–protein interactions. *Biointerphases*. 2017;12:02D404.
48. Ma Y, Wu Y, Lee JG, He L, Rother G, Fameau AL, et al. Adsorption of fatty acid molecules on amine-functionalized silica nanoparticles: surface organization and foam stability. *Langmuir*. 2020;36:3703–12.
49. May KL, Pham AC, Ramirez G, Herrera-Hidalgo C, Naeem Iqbal M, Robert-Nicoud G, et al. Towards mesoporous silica as a pharmaceutical treatment for obesity - impact on lipid digestion and absorption. *Eur J Pharm Biopharm*. 2022;173:1–11.
50. Guo Z, Martucci NJ, Liu Y, Yoo E, Tako E, Mahler GJ. Silicon dioxide nanoparticle exposure affects small intestine function in an in vitro model. *Nanotoxicology*. 2018;12:485–508.
51. Nassir F, Rector RS, Hammoud GM, Ibdah JA. Pathogenesis and prevention of hepatic steatosis. *Gastroenterol Hepatol*. 2015;11:167–75.
52. Francque SM, Marchesini G, Kautz A, Walmsley M, Dorner R, Lazarus JV, et al. Non-alcoholic fatty liver disease: A patient guideline. *JHEP Rep*. 2021;3:100322.
53. Jia X, Wang S, Zhou L, Sun L. The potential liver, brain, and embryo toxicity of titanium dioxide nanoparticles on mice. *Nanoscale Res Lett*. 2017;12:478.
54. Cui Y, Gong X, Duan Y, Li N, Hu R, Liu H, et al. Hepatocyte apoptosis and its molecular mechanisms in mice caused by titanium dioxide nanoparticles. *J Hazard Mater*. 2010;183:874–80.
55. Deng Y, Zhang Y, Lemos B, Ren H. Tissue accumulation of microplastics in mice and biomarker responses suggest widespread health risks of exposure. *Sci Rep*. 2017;7:46687.
56. Bao S, Tang W, Fang T. Sex-dependent and organ-specific toxicity of silver nanoparticles in livers and intestines of adult zebrafish. *Chemosphere*. 2020;249:126172.
57. Serflippi LM, Pallman DR, Russell B. Serum clinical chemistry and hematology reference values in outbred stocks of albino mice from three commonly used vendors and two inbred strains of albino mice. *Contemp Top Lab Anim*. 2003;42:46–52.
58. Mukai M, Ozasa K, Hayashi K, Kawai K. Various S-GOT/S-GPT ratios in non-viral liver disorders and related physical conditions and Life-Style. *Digest Dis Sci*. 2002;47:549–55.
59. Zhang Y, Li K, Kong A, Zhou Y, Chen D, Gu J, et al. Dysregulation of autophagy acts as a pathogenic mechanism of non-alcoholic fatty liver disease (NAFLD) induced by common environmental pollutants. *Ecotox Environ Safe*. 2021;217:112256.
60. Sun S, Yang Q, Zhou Q, Cao W, Yu S, Zhan S, et al. Long-term exposure to air pollution, habitual physical activity and risk of non-alcoholic fatty liver disease: A prospective cohort study. *Ecotox Environ Safe*. 2022;235:113440.
61. Ahmad J, Ahamed M, Akhtar MJ, Alokayan SA, Siddiqui MA, Musarrat J, et al. Apoptosis induction by silica nanoparticles mediated through reactive oxygen species in human liver cell line HepG2. *Toxicol Appl Pharm*. 2012;259:160–8.
62. Passagne I, Morille M, Rousset M, Pujalte I, L'Azou B. Implication of oxidative stress in size-dependent toxicity of silica nanoparticles in kidney cells. *Toxicology*. 2012;299:112–24.
63. Lai JC, Ananthakrishnan G, Jandhyam S, Dukhande VV, Bhushan A, Gokhale M, et al. Treatment of human astrocytoma U87 cells with silicon dioxide nanoparticles lowers their survival and alters their expression of mitochondrial and cell signaling proteins. *Int J Nanomedicine*. 2010;5:715–23.
64. Okoturo-Evans O, Dybowska A, Valsami-Jones E, Cupitt J, Gierula M, Boobis AR, et al. Elucidation of toxicity pathways in lung epithelial cells induced by silicon dioxide nanoparticles. *PLoS One*. 2013;8:e72363.
65. Gong C, Tao G, Yang L, Liu J, Liu Q, Zhuang Z. SiO<sub>2</sub> nanoparticles induce global genomic hypomethylation in HaCat cells. *Biochem Bioph Res Co*. 2010;397:397–400.
66. Yuan B, Zhang H, Wang X, Pan Y, Jiang J. Effect of nano-SiO<sub>2</sub> on expression and aberrant methylation of imprinted genes in lung and testis. *Nanoscale Res Lett*. 2018;13:266.
67. Pogribna M, Hammons G. Epigenetic effects of nanomaterials and nanoparticles. *J Nanobiotechnol*. 2021;19:2.
68. Ratziv V, Harrison SA, Francque S, Bedossa P, Leher P, Serfaty L, et al. Elafibranor, an agonist of the peroxisome proliferator-activated receptor- $\alpha$  and - $\delta$ , induces resolution of nonalcoholic steatohepatitis without fibrosis worsening. *Gastroenterology*. 2016;150:1147–59.
69. Chalasani N, Abdelmalek MF, Garcia-Tsao G, Vuppalanchi R, Alkhoufi N, Rinella M, et al. Effects of belataceptin, an inhibitor of galectin-3, in patients with nonalcoholic steatohepatitis with cirrhosis and portal hypertension. *Gastroenterology*. 2020;158:1334–45.
70. Harrison SA, Wong VWS, Okanoue T, Bzowej N, Vuppalanchi R, Younes Z, et al. Selonsertib for patients with bridging fibrosis or compensated cirrhosis due to NASH: Results from randomized phase III STELLAR trials. *J Hepatol*. 2020;73:26–39.
71. Sanyal AJ, Chalasani N, Kowdley KV, McCullough A, Diehl AM, Bass NM, et al. Pioglitazone, vitamin E, or placebo for nonalcoholic steatohepatitis. *New Eng J Med*. 2010;362:1675–85.
72. Mahmoud AM, Desouky EM, Hozayen WG, Bin-Jumah M, El-Nahass ES, Soliman HA, et al. Mesoporous silica nanoparticles trigger liver and kidney injury and fibrosis via altering TLR4/NF- $\kappa$ B, JAK2/STAT3, and Nrf2/HO-1 signaling in rats. *Biomolecules*. 2019;9:528.
73. Duan Y, Pan X, Luo J, Xiao X, Li J, Bestman PL, et al. Association of inflammatory cytokines with non-alcoholic fatty liver disease. *Front Immunol*. 2022;13:880298.
74. Lu CF, Yuan XY, Li LZ, Zhou W, Zhao J, Wang YM, et al. Combined exposure to nano-silica and lead induced potentiation of oxidative stress and DNA damage in human lung epithelial cells. *Ecotox Environ Safe*. 2015;122:537–44.
75. Podszun MC, Chung JY, Ylaya K, Kleiner DE, Hewitt SM, Rotman Y. 4-HNE immunohistochemistry and image analysis for detection of lipid peroxidation in human liver samples using vitamin E treatment in NAFLD as a proof of concept. *J Histochem Cytochem*. 2020;68:635–43.
76. Chen Z, Tian R, She Z, Cai J, Li H. Role of oxidative stress in the pathogenesis of nonalcoholic fatty liver disease. *Free Radical Bio Med*. 2020;152:116–41.
77. Birkenfeld AL, Shulman GI. Nonalcoholic fatty liver disease, hepatic insulin resistance, and type 2 Diabetes. *Hepatology*. 2014;59:713–23.
78. Nicholson JK, Lindon JC. Systems biology: Metabonomics. *Nature*. 2008;455:1054–6.
79. Hodson L, Gunn PJ. The regulation of hepatic fatty acid synthesis and partitioning: the effect of nutritional state. *Nat Rev Endocrinol*. 2019;15:689–700.

80. Pirola CJ, Sookoian S. Multiomics biomarkers for the prediction of non-alcoholic fatty liver disease severity. *World J Gastroenterol*. 2018;24:1601–15.
81. Shen J, Zhang J, Wen J, Ming Q, Zhang J, Xu Y. Correlation of serum alanine aminotransferase and aspartate aminotransferase with coronary heart disease. *INT J Clin Exp Med*. 2015;8:4399–404.
82. Raurich JM, Llompарт-Pou JA, Rodríguez-Yago M, Ferreruela M, Royo C, Ayestarán I. Role of Elevated Aminotransferases in ICU Patients with Rhabdomyolysis. *Am Surgeon*. 2015;81:1209–15.
83. Weng SF, Kai J, Guha IN, Qureshi N. The value of aspartate aminotransferase and alanine aminotransferase in cardiovascular disease risk assessment. *Open Heart*. 2015;2:e000272.
84. Henaо-Mejia J, Elinav E, Jin C, Hao L, Mehal WZ, Strowig T, et al. Inflammation-mediated dysbiosis regulates progression of NAFLD and obesity. *Nature*. 2012;482:179–85.
85. Schmidt-Arras D, Rose-John S. IL-6 pathway in the liver: From pathophysiology to therapy. *J Hepatol*. 2016;64:1403–15.
86. Kao J, Thorkelsson K, Bai P, Rancatore BJ, Xu T. Toward functional nanocomposites: taking the best of nanoparticles, polymers, and small molecules. *Chem Soc Rev*. 2013;42:2654–78.
87. Radin S, Falaize S, Lee MH, Ducheyne P. In vitro bioactivity and degradation behavior of silica xerogels intended as controlled release materials. *Biomaterials*. 2002;23:3113–22.
88. Francque S, Verrijken A, Caron S, Prawitt J, Paumelle R, Derudas B, et al. PPAR $\alpha$  gene expression correlates with severity and histological treatment response in patients with non-alcoholic steatohepatitis. *J Hepatol*. 2015;63:164–73.
89. Ip E, Farrell GC, Robertson G, Hall P, Kirsch R, Leclercq I. Central role of PPAR $\alpha$ -dependent hepatic lipid turnover in dietary steatohepatitis in mice. *Hepatology*. 2003;38:123–32.
90. Ito Y, Yanagiba Y, Ramdhan DH, Hayashi Y, Li Y, Suzuki AK, et al. Nanoparticle-rich diesel exhaust-induced liver damage via inhibited transactivation of peroxisome proliferator-activated receptor  $\alpha$ . *Environ Toxicol*. 2016;31:1985–95.
91. Yu DD, Van Citters G, Li H, Stoltz BM, Forman BM. Discovery of novel modulators for the PPAR $\alpha$  (peroxisome proliferator activated receptor  $\alpha$ ): Potential therapies for nonalcoholic fatty liver disease. *Bioorgan Med Chem*. 2021;41:116193.

## Publisher's Note

Springer Nature remains neutral with regard to jurisdictional claims in published maps and institutional affiliations.